Numerical Algorithms
https://doi.org/10.1007/s11075-023-01602-0

ORIGINAL PAPER

High-order half-step compact numerical approximation for fourth-order parabolic PDEs

Deepti Kaur[1] · R. K. Mohanty[2]

Received: 11 March 2022 / Accepted: 18 June 2023

Abstract

The aim of this study is to develop compact difference method to approximate parabolic PDEs of fourth order equipped with Dirichlet and Neumann boundary conditions involving half-step points. The proposed method converges quaternary and quadratically in space and time, respectively. The imbedding technique has been applied to approximate derivative terms of lower order by means of the governing differential equation to deduce the high-order method. The primary utility of this new discretization is that it can be straightaway applied to problems with singularities without necessitating fictitious nodes or special approach which has consequently lowered computational complicacy. We have examined linear stability of the proposed three-level implicit difference scheme using matrix stability analysis. In addition, we also obtained the solution of the first-order spatial derivative which is of significance in several physical problems. The efficacy of the proposed approximation is confirmed through numerical tests performed on a collection of physically relevant problems comprising the Euler Bernoulli beam equation and the highly nonlinear good Boussinesq equation. Numerical experiments evidently exhibit that the method provides more accurate results in contrast with the existing numerical techniques. The present method is able to simulate well the complex and intriguing long time dynamics of the good Boussinesq equation.

Keywords Fourth-order parabolic equations · Compact difference method · Euler-Bernoulli beam equation · Good Boussinesq equation · Solitary wave · Block tridiagonal

Mathematics Subject Classification (2010) 65M06 · 65M12 · 65M22

✉ R. K. Mohanty
rmohanty@sau.ac.in

Extended author information available on the last page of the article

1 Introduction

In this research, we consider the generalized form of one-dimensional fourth-order parabolic partial differential equations (PDEs):

$$a(x,t)\frac{\partial^4 v}{\partial x^4}+\frac{\partial^2 v}{\partial t^2}=\phi(x,t,v,v_t,v_x,v_{xx},v_{xxx}),\qquad (x,t)\in\Omega \tag{1}$$

with the initial conditions

$$v(x,0)=v_0(x),\quad x_a\le x\le x_b, \tag{2.1}$$

$$\frac{\partial v}{\partial t}(x,0)=v_1(x),\quad x_a\le x\le x_b. \tag{2.2}$$

The Dirichlet and Neumann boundary conditions are given by

$$v(x_a,t)=f_0(t),\qquad v(x_b,t)=g_0(t),\quad t>0, \tag{3.1}$$

$$\frac{\partial v}{\partial x}(x_a,t)=f_1(t),\quad \frac{\partial v}{\partial x}(x_b,t)=g_1(t),\quad t>0, \tag{3.2}$$

where $\Omega\equiv(x_a,x_b)\times(0,\infty)$ and the functions ϕ, v_0, v_1, f_0, g_0, f_1, g_1 are sufficiently smooth real valued functions. We have presumed that the solution $v(x,t)$ is smooth enough so that the order and accuracy of the underlying finite difference method is preserved. Fourth-order PDEs of type (1) model various phenomenally significant problems in scientific and engineering disciplines like fluid flow, shallow water waves, vibrations of a homogenous beam, deformation of beams, ion-acoustic wave in plasma, magnetohydrodynamics wave in plasma, and pressure wave in liquid–gas bubble mixtures [3, 12, 20].

The class of PDEs (1) admits, in specific, the *Euler-Bernoulli beam equation* that governs the transverse vibrations of a beam [26]:

$$\rho A(x)\frac{\partial^2 v}{\partial t^2}+\frac{\partial^2}{\partial x^2}\left(EI(x)\frac{\partial^2 v}{\partial x^2}\right)=0, \tag{4}$$

where $0<x<l$, l is length of the beam, $t>0$, ρ is the beam material density, $A(x)$ is the beam cross-section area, and $EI(x)>0$ is the flexural rigidity or bending stiffness of the beam. This is the oldest though commonly applied model describing the motion of an inextensible beam with the neutral axis along the x-axis. The support position of the ends of the beam determines the boundary conditions corresponding to Eq. (4). For instance, the boundary conditions corresponding to a beam whose each end is clamped or whose one end is clamped and other end is free occur physically in the study of fourth-order problems. A beam that is clamped at both ends corresponds to boundary conditions of the type (3.1)–(3.2). The Euler-Bernoulli model is yielded by the classical linear theory of deformation. The first coherent theory of elasticity of thin beams was formulated by Jacob Bernoulli wherein the curvature at any point of an elastic beam is proportionately related to the bending moment of that point.

Furthermore, a PDE was derived for the displacement of a thin vibrating beam [12] which is based on his uncle's theory of elasticity. Afterwards, Bernoulli's theory was extended and applied to the loaded beams [26] by Leonard Euler. The Bernoulli's beam equation solution is significant in numerous areas of engineering, for instance, in the production of flexible frameworks (buildings and railway construction) and in the layout of robotic designs. The vibration of beams has been studied extensively in the past and is still of interest to scientists and engineers. For analyzing the underlying model for the motion of a beam, we refer to [12, 20].

Another significant example is the *good Boussinesq equation* that is analogous to the Korteweg-de Vries equation and nonlinear Schödinger equation presenting a balance between dispersion and nonlinearity which leads to the soliton solutions [4]. The nonlinear good Boussinesq equation was first derived by Boussinesq [3] and has the following form:

$$\frac{\partial^2 v}{\partial t^2} = \frac{\partial^2 v}{\partial x^2} + \frac{\partial^2 (v^2)}{\partial x^2} - \frac{\partial^4 v}{\partial x^4}. \tag{5}$$

The nonlinear Boussinesq equation (5) is another significant model which has varied applications in diverse fields, such as longitudinal dispersive wave in elastic rods, magnetohydrodynamics wave in plasma, pressure wave in liquid–gas bubble mixtures, and ion-acoustic wave in plasma (see [4, 19]). It represents shallow water waves progressing in both directions and exhibits an extremely complex mechanism of solitary wave association (see [3, 10] and references therein).

There exist extensive literature on numerical study of fourth-order parabolic PDEs and still undergoing recent developments which has resulted in numerous research articles in this area. In the past, Sinc discretization for the fourth-order spatial problem and the second-order temporal problem was presented with various common boundary conditions by Smith et al. [25]. Mohammadi [21] proposed a collocation method based on sextic B-spline basis for the Euler-Bernoulli problems with fixed and cantilever boundary conditions emerging in robotic layouts. Later, El-Gamel [11] investigated fourth-order PDE with variable coefficients modeling the transverse vibrations of a uniform flexible beam using sinc-Galerkin method and obtained accurate results even though singularities exist at the boundaries. In recent years, fourth-order accurate in space and second-order accurate in time two-level implicit difference formulas employing only three, nine, and nineteen spatial nodes for one-, two-, and three-dimensional vibration problems, respectively, of a single compact stencil were developed in [22]. In contrast to their linear counterparts, it is quite challenging to solve numerically nonlinear PDEs such as the good Boussinesq equation due to its complex principle of solitary wave collaboration. The good Boussinesq equation has been extensively studied and analyzed in literature. Earlier, Manoranjan et al. [18] obtained an analytic formula for the two-soliton interaction using Petrov-Galerkin method. Numerical study of Boussinesq equation can be traced back to the work of Bratsos [4] wherein finite difference method was developed using method of lines. Later, Bratsos [5] applied a predictor-corrector scheme based on rational approximants for the numerical solution of good Boussinesq equation. Mohebbi and Asgari [1] numerically solved (5) with fourth-order time-stepping schemes in combination with discrete Fourier transform. Afterwards, Dehghan and Salehi [10] employed the boundary-only meshfree method for the classical Boussinesq equation in one dimension. A highly accurate finite difference method by transforming (5) into a first-order differential system in time has been proposed in [14]. High-order energy preserving scheme is obtained for the good Bossinesq equation by pseudo-spectral method in spatial variable and the fourth-order average vector field method in time variable in [15]. Yan and Zhang [30] discretized the good Boussinesq equation in space using the Fourier pseudospectral method and in time by applying the Hamiltonian boundary value method to construct energy conserving schemes. Furthermore, Zhang et al. [31] designed two numerical methods for solving the spatial-temporal pseudo-spectral collocation formulations for the good Boussinesq equation by applying Krylov deferred correction method in one time-marching step. The standard finite difference method was improved to construct highly efficient structure-preserving methods for the good Boussinesq equation by Chen et al. [9]. Lately, Ostermann and Su [23] introduced two exponential-type integrators of orders one and two, respectively, for the good Boussinesq equation. Brugnano et al. [6] studied the good Boussinesq equation for the geometric numerical solution by applying a spectrally accurate Fourier space semi-discretization. The moving mesh method and the He semiinverse approach have been employed to determine the numerical and soliton solutions, respectively, for the good Boussinesq equation in [2]. Recently, Su and Yao [27] considered a second-order Deuflhard-type exponential integrator Fourier pseudo-spectral method for solving the good Boussinesq equation. Ucar et al. [28] constructed Galerkin finite element model based on cubic basis for the Boussinesq type equations.

The fourth-order parabolic PDEs poses numerous challenges which are of less concern to the first- and second-order equations when applying finite differences for the numerical solution. The accuracy in that case relies on the approximations employed at the boundary. Time stepping is also crucial for these equations. The available fourth-order accurate in space implicit difference formula of [16] for parabolic problems of fourth order uses three spatial grid points but is unable to determine the solution at singular points because of the presence of the terms of the form $1/x_{l-1}$ that creates difficulties at $l = 1$ where $x_0 = 0$, thus requires particular handling for solving singular problems resulting in tiresome calculations. In the present work, by considering solution values v and $\partial v/\partial x$ at each node, we develop difference scheme based on half-step discretization for solving fourth-order evolution equations using same number of nodes. The proposed method involve the terms like $1/x_{l-1/2}$ instead of $1/x_{l-1}$ and hence considerably more advantageous to apply at $x = 0$. Thus, the present approach employs half-step nodes like the discretization devised for a two-point boundary-value problem by Chawla and Shivakumar [8] and is therefore called the *half-step discretization*. The proposed method stems from a sort combination of the methods proposed in [16] and [8], which is applicable to solve both singular and non-singular problems, and in such a combination lies the main contribution of the manuscript.

The paper is organized as follows. In Sect. 2, we formulate and derive the compact difference scheme based on half-step discretization of order four in space and two in time for the PDE (1). The stability of the derived three-level difference scheme has been examined by the matrix method for a linear problem in Sect. 3. Some numerical experiments are reported in Sect. 4 to corroborate the accuracy and effectiveness of the new method. We have compared our results with the previously developed methods for the physical problems such as the Euler-Bernoulli beam equation [21] and the highly nonlinear good Boussinesq equation [5–7, 10, 14, 28, 29]. Numerical findings exhibit that the derived solutions not only approximate the analytical solutions very closely but are also more accurate than those derived using the existing methods [5–7, 10, 14, 21, 28, 29]. Finally, some remarks are summarized in Sect. 5 based on theoretical findings and numerical experiments.

2 Formulation and derivation of compact difference scheme

This section is devoted to introduce the idea for constructing our new finite difference method. Considering the prescribed boundary data, the solution values $v(x,t)$ and its spatial derivative of first order $w(x,t) = \frac{\partial v}{\partial x}(x,t)$ are employed for deriving highly accurate compact difference method for the parabolic PDE (1) of fourth order.

We discretize the solution domain Ω with mesh sizes $h > 0$ and $\tau > 0$ in the x- and t- directions, respectively. The grid points (x_l, t_k) are given by $x_l = x_a + lh$ and $t_k = k\tau$, where $l = 0, 1, \ldots, N+1$, $k = 0, 1, 2, \ldots$; N being a positive integer with $(N+1)h = x_b - x_a$. Let $\lambda = (\tau/h^2) > 0$ denotes the mesh ratio parameter. Let V_l^k and W_l^k be the exact solution values of the functions $v(x,t)$ and $w(x,t)$ at the node (x_l, t_k), respectively. The approximation of the functions $v(x,t)$ and $w(x,t)$ at the same node is denoted by v_l^k and w_l^k, respectively.

At the grid point (x_l, t_k), for $S = V$ and W, we denote

$$S_{rs} = \frac{\partial^{r+s} S}{\partial x^r \partial t^s}, \quad r, s = 0, 1, \ldots.$$

For understanding the formation of the method, we first consider the following ordinary differential equation of fourth order:

$$a(x)\frac{d^4 v}{dx^4} = \phi(x), \qquad x_a < x < x_b \tag{6}$$

with v and $w = \frac{dv}{dx}$ specified along the boundary.

By the help of Taylor series expansion, we can easily verify that

$$V_{l+1} + V_{l-1} = 2V_l + h^2\left(\frac{d^2 V}{dx^2}\right)_l + \frac{h^4}{12}\left(\frac{d^4 V}{dx^4}\right)_l + \frac{h^6}{360}\left(\frac{d^6 V}{dx^6}\right)_l + O(h^8) \tag{7.1}$$

$$V_{l+1} - V_{l-1} = 2hV_{x_l} + \frac{h^3}{3}\left(\frac{d^3 V}{dx^3}\right)_l + \frac{h^5}{60}\left(\frac{d^5 V}{dx^5}\right)_l + O(h^7) \tag{7.2}$$

$$h(W_{l+1} + W_{l-1}) = 2hV_{x_l} + h^3\left(\frac{d^3 V}{dx^3}\right)_l + \frac{h^5}{12}\left(\frac{d^5 V}{dx^5}\right)_l + O(h^7) \tag{7.3}$$

$$h(W_{l+1} - W_{l-1}) = 2h^2\left(\frac{d^2 V}{dx^2}\right)_l + \frac{h^4}{3}\left(\frac{d^4 V}{dx^4}\right)_l + \frac{h^6}{60}\left(\frac{d^6 V}{dx^6}\right)_l + O(h^8) \tag{7.4}$$

Eliminating $\left(\frac{d^2V}{dx^2}\right)_l$ from (7.1) and (7.4), we obtain (8.1). Likewise, eliminating $\left(\frac{d^3V}{dx^3}\right)_l$ from (7.2) and (7.3), we obtain (8.2):

$$h^4\left(\frac{d^4V}{dx^4}\right)_l = -12(V_{l-1}-2V_l+V_{l+1})+6h(W_{l+1}-W_{l-1})-\frac{h^6}{15}\left(\frac{d^6V}{dx^6}\right)_l+O(h^8), \tag{8.1}$$

$$h^5\left(\frac{d^5V}{dx^5}\right)_l = -90(V_{l+1}-V_{l-1})+30h(W_{l-1}+4W_l+W_{l+1})+O(h^7),\quad l=1,\ldots,N \tag{8.2}$$

Above are the finite difference approximations for the derivatives in terms of the function values v and w involving only three nodes of a single compact stencil.

For deriving the high-order compact approximation, we consider the linear combination and use the governing differential (6) to obtain

$$\begin{aligned}
&h^4(P_0\phi_l+hP_1\phi_{x_l}+h^2P_2\phi_{xx_l})\\
&=h^4P_0a_l\left(\frac{d^4V}{dx^4}\right)_l+h^5P_1\left[a_l\left(\frac{d^5V}{dx^5}\right)_l+a_{x_l}\left(\frac{d^4V}{dx^4}\right)_l\right]\\
&+h^6P_2\left[a_l\left(\frac{d^6V}{dx^6}\right)_l+2a_{x_l}\left(\frac{d^5V}{dx^5}\right)_l+a_{xx_l}\left(\frac{d^4V}{dx^4}\right)_l\right]\\
&=\left(a_lP_0+ha_{x_l}P_1+h^2a_{xx_l}P_2\right)h^4\left(\frac{d^4V}{dx^4}\right)_l+\left(a_lP_1+2ha_{x_l}P_2\right)h^5\left(\frac{d^5V}{dx^5}\right)_l\\
&+a_lP_2h^6\left(\frac{d^6V}{dx^6}\right)_l
\end{aligned} \tag{9}$$

where P_0, P_1, P_2 are real constants to be calculated and $\phi_l=\phi(x_l)$, $a_l=a(x_l)$ and so on. Employing the approximation (8.1) in (9) leads to

$$\begin{aligned}
&h^4(P_0\phi_l+hP_1\phi_{x_l}+h^2P_2\phi_{xx_l})\\
&=\left(a_lP_0+ha_{x_l}P_1+h^2a_{xx_l}P_2\right)\left[-12(V_{l-1}-2V_l+V_{l+1})+6h(W_{l+1}-W_{l-1})-\frac{h^6}{15}\left(\frac{d^6V}{dx^6}\right)_l\right]\\
&+\left(a_lP_1+2ha_{x_l}P_2\right)h^5\left(\frac{d^5V}{dx^5}\right)_l+a_lP_2h^6\left(\frac{d^6V}{dx^6}\right)_l+O(h^8)
\end{aligned} \tag{10}$$

For the fourth-order compact difference method, we equate the coefficients of $h^5\left(\frac{d^5V}{dx^5}\right)_l$ and $h^6\left(\frac{d^6V}{dx^6}\right)_l$ to zero in (10) to obtain

$$P_1=-2h\frac{a_{x_l}}{a_l}P_2,\quad P_0=15P_2$$

Let $P_2=1$, we have $P_0=15$ and $P_1=-2h\frac{a_{x_l}}{a_l}$.

We approximate the derivatives in (10) by second-order finite difference method using half-step points:

$$\phi_{x_l} = \frac{\phi_{l+\frac{1}{2}} - \phi_{l-\frac{1}{2}}}{h} + O(h^2), \tag{11.1}$$

$$\phi_{xx_l} = \frac{4\left(\phi_{l-\frac{1}{2}} - 2\phi_l + \phi_{l+\frac{1}{2}}\right)}{h^2} + O(h^2), \tag{11.2}$$

where $\phi_{l\pm\frac{1}{2}} = \phi(x_{l\pm\frac{1}{2}})$, $x_{l\pm\frac{1}{2}} = x_l \pm \frac{h}{2}$. Using the above approximations and the obtained parameters in (10), it yields the fourth-order compact difference method for (6):

$$\begin{aligned}&\left[a_l - \frac{2h^2}{15}\frac{a_{x_l}}{a_l}a_{x_l} + \frac{h^2}{15}a_{xx_l}\right]\left[-2(V_{l-1} - 2V_l + V_{l+1}) + h(W_{l+1} - W_{l-1})\right]\\ &= \frac{h^4}{90}\left[\left(4 + 2h\frac{a_{x_l}}{a_l}\right)\phi_{l-\frac{1}{2}} + 7\phi_l + \left(4 - 2h\frac{a_{x_l}}{a_l}\right)\phi_{l+\frac{1}{2}}\right] + O(h^8), \quad l = 1, \ldots, N\end{aligned} \tag{12}$$

Analogously, to derive the compact difference approximation of fourth order for $w(x)$, the following linear combination is considered:

$$\begin{aligned}&h^4(R_0\phi_l + hR_1\phi_{x_l} + h^2R_2\phi_{xx_l})\\ &= \left(a_lR_0 + ha_{x_l}R_1 + h^2a_{xx_l}R_2\right)h^4\left(\frac{d^4V}{dx^4}\right)_l + \left(a_lR_1 + 2ha_{x_l}R_2\right)h^5\left(\frac{d^5V}{dx^5}\right)_l\\ &\quad + a_lR_2h^6\left(\frac{d^6V}{dx^6}\right)_l\end{aligned} \tag{13}$$

where R_0, R_1 and R_2 are the unknowns to be suitably determined. Employing the approximation (8.2) in (13), we obtain

$$\begin{aligned}&h^4(R_0\phi_l + hR_1\phi_{x_l} + h^2R_2\phi_{xx_l})\\ &\quad= \left(a_lR_0 + ha_{x_l}R_1 + h^2a_{xx_l}R_2\right)h^4\left(\frac{d^4V}{dx^4}\right)_l\\ &\qquad + \left(a_lR_1 + 2ha_{x_l}R_2\right)\left[-90(V_{l+1} - V_{l-1}) + 30h(W_{l-1} + 4W_l + W_{l+1})\right]\\ &\qquad + a_lR_2h^6\left(\frac{d^6V}{dx^6}\right)_l + O(h^7)\end{aligned} \tag{14}$$

For the fourth-order compact approximation of $w(x)$, we equate the coefficients of $h^4\left(\frac{d^4V}{dx^4}\right)_l$ and $h^6\left(\frac{d^6V}{dx^6}\right)_l$ to zero in (14) to obtain

$$a_lR_0 + ha_{x_l}R_1 + h^2a_{xx_l}R_2 = 0, \quad R_2 = 0$$

Let $R_1 = 1$, we get $R_0 = -h\frac{a_{x_l}}{a_l}$. Substituting the values of R_0, R_1, R_2 back in (14) and applying the approximation (11.1) leads to the following $O(h^4)$ accurate discretization for $w(x)$:

$$\begin{aligned}
&a_l\left[-3(V_{l+1}-V_{l-1})+h(W_{l-1}+4W_l+W_{l+1})\right]\\
&\quad=\frac{h^4}{30}\left[\phi_{l+\frac{1}{2}}-\phi_{l-\frac{1}{2}}-h\left(\frac{a_{x_l}}{a_l}\right)\phi_l\right]+O(h^7),\\
&l=1,\ldots,N
\end{aligned}\tag{15}$$

Now, we develop the approximations (12) and (15) for the initial boundary value problem (1) comprising higher order derivatives. This is accomplished by defining appropriate approximations to v, w, v_t, v_{tt}, v_{xx}, w_{xx} at the node (x_l, t_k) and the adjacent half-step nodes $(x_{l\pm\frac{1}{2}}, t_k)$. For the higher-order method, we consider the below approximations denoted by "$\widehat{\cdot}$" for the respective solution variables and their partial derivatives. For $r = 0, \pm 1$, we let

$$\widehat{V}^k_{l+r} = \eta V^{k+1}_{l+r} + (1-2\eta)V^k_{l+r} + \eta V^{k-1}_{l+r}, \quad 0<\eta<1 \tag{16.1}$$

$$\widehat{W}^k_{l+r} = \eta W^{k+1}_{l+r} + (1-2\eta)W^k_{l+r} + \eta W^{k-1}_{l+r}, \quad 0<\eta<1 \tag{16.2}$$

$$(\widehat{V}_t)^k_{l+r} = (V^{k+1}_{l+r} - V^{k-1}_{l+r})/(2\tau), \tag{16.3}$$

$$(\widehat{V}_{tt})^k_{l+r} = (V^{k+1}_{l+r} - 2V^k_{l+r} + V^{k-1}_{l+r})/\tau^2, \tag{16.4}$$

$$\widehat{V}^k_{l\pm\frac{1}{2}} = \frac{1}{2}(\widehat{V}^k_{l\pm1} + \widehat{V}^k_l), \tag{16.5}$$

$$(\widehat{V}_t)^k_{l\pm\frac{1}{2}} = \frac{1}{4\tau}(V^{k+1}_{l\pm1} + V^{k+1}_l - V^{k-1}_{l\pm1} - V^{k-1}_l), \tag{16.6}$$

$$\widehat{W}^k_{l\pm\frac{1}{2}} = \pm\frac{1}{h}(\widehat{V}^k_{l\pm1} - \widehat{V}^k_l), \tag{16.7}$$

$$(\widehat{V}_{xx})^k_l = (\widehat{W}^k_{l+1} - \widehat{W}^k_{l-1})/(2h), \tag{16.8}$$

$$(\widehat{V}_{xx})^k_{l\pm\frac{1}{2}} = \pm\frac{1}{h}(\widehat{W}^k_{l\pm1} - \widehat{W}^k_l), \tag{16.9}$$

$$(\widehat{W}_{xx})^k_l = (\widehat{W}^k_{l+1} - 2\widehat{W}^k_l + \widehat{W}^k_{l-1})/h^2. \tag{16.10}$$

We define the functional approximation:

$$\begin{aligned}
\widehat{\Phi}^k_l &= \phi\left(x_l, t_k, \widehat{V}^k_l, (\widehat{V}_t)^k_l, \widehat{W}^k_l, (\widehat{V}_{xx})^k_l, (\widehat{W}_{xx})^k_l\right)\\
&= \Phi^k_l + O(\tau^2 + h^2),
\end{aligned}\tag{17}$$

where $\Phi^k_l = \phi(x_l, t_k, V^k_l, V^k_{t_l}, W^k_l, V^k_{xx_l}, W^k_{xx_l})$. For $O(\tau^2 + h^2)$ approximation of w_{xx} at the half-step points $(x_{l\pm1/2}, t_k)$, consider the following linear combination:

$$\begin{aligned}
h^3(\widehat{W}_{xx})^k_{l\pm\frac{1}{2}} &= \alpha_0(\widehat{V}^k_{l+1} - \widehat{V}^k_{l-1} - 2h\widehat{W}^k_l) + \alpha_1(\widehat{V}^k_{l+1} + \widehat{V}^k_{l-1} - 2\widehat{V}^k_l) + \alpha_2 h(\widehat{W}^k_{l+1} - \widehat{W}^k_{l-1})\\
&= h^3 W^k_{xx_{l\pm\frac{1}{2}}} + O(\tau^2h^3 + h^5)
\end{aligned}\tag{18}$$

where α_0, α_1 and α_2 are the real constants to be calculated. By Taylor series expansion, we have

$$\alpha_0 \frac{h^3}{3}\left(\frac{\partial^3 V}{\partial x^3}\right)_l^k + \alpha_1\left[h^2 V_{xx_l}^k + \frac{h^4}{12}\left(\frac{\partial^4 V}{\partial x^4}\right)_l^k\right] + \alpha_2\left[2h^2 V_{xx_l}^k + \frac{h^4}{3}\left(\frac{\partial^4 V}{\partial x^4}\right)_l^k\right]$$
$$= h^3\left(\frac{\partial^3 V}{\partial x^3}\right)_l^k \pm \frac{h^4}{2}\left(\frac{\partial^4 V}{\partial x^4}\right)_l^k + O(\tau^2 h^3 + h^5)$$

Equating the coefficients up to h^4 to zero in above, we obtain $(\alpha_0, \alpha_1, \alpha_2) = (3, \mp 6, \pm 3)$. Thus, we have the approximations:

$$\begin{aligned}(\widehat{W}_{xx})_{l\pm\frac{1}{2}}^k &= \frac{3}{h^3}(\widehat{V}_{l+1}^k - \widehat{V}_{l-1}^k - 2h\widehat{W}_l^k) \mp \frac{6}{h^3}(\widehat{V}_{l+1}^k + \widehat{V}_{l-1}^k - 2\widehat{V}_l^k) \pm \frac{3}{h^2}(\widehat{W}_{l+1}^k - \widehat{W}_{l-1}^k)\\ &= W_{xx_{l\pm\frac{1}{2}}}^k + O(\tau^2 + h^2)\end{aligned} \tag{19}$$

Next, we define the functional approximation:

$$\widehat{\Phi}_{l\pm\frac{1}{2}}^k = \phi\left(x_{l\pm\frac{1}{2}}, t_k, \widehat{V}_{l\pm\frac{1}{2}}^k, (\widehat{V}_t)_{l\pm\frac{1}{2}}^k, \widehat{W}_{l\pm\frac{1}{2}}^k, (\widehat{V}_{xx})_{l\pm\frac{1}{2}}^k, (\widehat{W}_{xx})_{l\pm\frac{1}{2}}^k\right) \tag{20}$$

Employing $O(\tau^2 + h^2)$ approximations (16.5)-(16.7), (16.9) and (19) in (20), we get

$$\begin{aligned}\widehat{\Phi}_{l\pm\frac{1}{2}}^k &= \phi\Big(x_l, t_k, V_{l\pm\frac{1}{2}}^k + W_{l\pm\frac{1}{2}}^k + O(\tau^2 + h^2), V_{xx_{l\pm\frac{1}{2}}}^k + O(\tau^2 + h^2)\,,\\ &\qquad O(\tau^2 + h^2), V_{t_{l\pm\frac{1}{2}}}^k + O(\tau^2 + h^2), W_{xx_{l\pm\frac{1}{2}}}^k + O(\tau^2 + h^2)\Big)\\ &= \Phi_{l\pm\frac{1}{2}}^k + O(\tau^2 + h^2)\end{aligned} \tag{21}$$

where $\Phi_{l\pm\frac{1}{2}}^k = \phi\left(x_l, t_k, V_{l\pm\frac{1}{2}}^k, V_{t_{l\pm\frac{1}{2}}}^k, W_{l\pm\frac{1}{2}}^k, V_{xx_{l\pm\frac{1}{2}}}^k, W_{xx_{l\pm\frac{1}{2}}}^k\right)$. For the higher order method, we require additional approximations to the second-order partial derivatives of the solution variables $v(x,t)$ and $w(x,t)$ at the central node (x_l, t_k) and neighboring half-step points $(x_{l\pm\frac{1}{2}}, t_k)$ denoted by "$\widehat{\widehat{\cdot}}$" for the respective solution variables. Consider the following linear combination:

$$\begin{aligned}h^2(\widehat{\widehat{V}}_{xx})_l^k &= \alpha_{10}(\widehat{V}_{l+1}^k + \widehat{V}_{l-1}^k - 2\widehat{V}_l^k) + \alpha_{11}h(\widehat{W}_{l+1}^k - \widehat{W}_{l-1}^k)\\ &= h^2 V_{xx_l}^k + O(\tau^2 h^2 + h^6)\end{aligned} \tag{22}$$

where α_{10} and α_{11} are real constants to be found suitably. With the aid of Taylors expansion, we have

$$\alpha_{10}\left(h^2V^k_{xx_l}+\frac{h^4}{12}\left(\frac{\partial^4 V}{\partial x^4}\right)^k_l\right)+\alpha_{11}\left(2h^2V^k_{xx_l}+\frac{h^4}{3}\left(\frac{\partial^4 V}{\partial x^4}\right)^k_l\right)=h^2V^k_{xx_l}+O(\tau^2h^2+h^6)$$

Equating the coefficients up to h^4 to zero in above, we get

$$\alpha_{10}=2,\quad \alpha_{11}=-\frac{1}{2}.$$

Thus, we have the approximation:

$$(\widehat{\widehat{V}}_{xx})^k_l=\frac{2}{h^2}(\widehat{V}^k_{l-1}-2\widehat{V}^k_l+\widehat{V}^k_{l+1})-\frac{1}{2h}(\widehat{W}^k_{l+1}-\widehat{W}^k_{l-1})=V^k_{xx_l}+O(\tau^2+h^4)\quad(23)$$

Similarly, we obtain the following approximation:

$$(\widehat{\widehat{W}}_{xx})^k_l=\frac{15}{2h^3}(\widehat{V}^k_{l+1}-\widehat{V}^k_{l-1})-\frac{3}{2h^2}(\widehat{W}^k_{l-1}+8\widehat{W}^k_l+\widehat{W}^k_{l+1})=W^k_{xx_l}+O(\tau^2+h^4)\quad(24)$$

Using the additional approximations to the second-order spatial derivatives, we define the functional approximation at the central node (x_l, t_k) by

$$\widehat{\widehat{\Phi}}^k_l=\phi\left(x_l,t_k,\widehat{V}^k_l,(\widehat{V}_t)^k_l,\widehat{W}^k_l,(\widehat{\widehat{V}}_{xx})^k_l,(\widehat{\widehat{W}}_{xx})^k_l\right)=\Phi^k_l+O(\tau^2+h^4)\qquad(25)$$

Further, in addition the following higher order approximations at half-step nodes $(x_{l\pm\frac{1}{2}}, t_k)$ are considered:

$$\widehat{\widehat{V}}^k_{l\pm\frac{1}{2}}=\frac{1}{2}(\widehat{V}^k_{l\pm1}+\widehat{V}^k_l)-\frac{h}{16}(\widehat{W}^k_{l+1}-\widehat{W}^k_{l-1})=V^k_{l\pm\frac{1}{2}}+\eta\tau^2V_{02}+O(\tau^2h+\tau^2h^2+h^3),\qquad(26.1)$$

$$(\widehat{\widehat{V}}_t)^k_{l\pm\frac{1}{2}}=\frac{1}{2}(\widehat{V}^k_{t_{l\pm1}}+\widehat{V}^k_{t_l})-\frac{h}{32\tau}(W^{k+1}_{l+1}+W^{k-1}_{l-1}-W^{k-1}_{l+1}-W^{k+1}_{l-1})$$
$$=V^k_{t_{l\pm\frac{1}{2}}}+\frac{\tau^2}{6}V_{03}+O(\tau^2h+\tau^2h^2+h^3),\qquad(26.2)$$

$$\widehat{\widehat{W}}^k_{l\pm\frac{1}{2}}=\frac{1}{2}(\widehat{W}^k_{l\pm1}+\widehat{W}^k_l)-\frac{1}{8}(\widehat{W}^k_{l+1}-2\widehat{W}^k_l+\widehat{W}^k_{l-1})=W^k_{l\pm\frac{1}{2}}+\eta\tau^2V_{12}+O(\tau^2h+\tau^2h^2+h^3),\qquad(26.3)$$

For the high-order approximation of v_{xx} and w_{xx} at the half-step points, we let

$$h^2(\widehat{\widehat{V}}_{xx})^k_{l+\frac{1}{2}}=\gamma_0(\widehat{V}^k_{l+1}-2\widehat{V}^k_l+\widehat{V}^k_{l-1})+\gamma_1h(\widehat{W}^k_{l+1}-\widehat{W}^k_{l-1})+\gamma_2(\widehat{V}^k_{l+1}-\widehat{V}^k_{l-1}-2h\widehat{W}^k_l)$$
$$=h^2V^k_{xx_{l+\frac{1}{2}}}+O(\tau^2h^3+h^5)\qquad(27)$$

Expanding the right-hand side of (27) about (x_l, t_k) using Taylor series and equating the coefficients upto h^4 to zero, we obtain $(\gamma_0, \gamma_1, \gamma_2) = (\frac{1}{2}, \frac{1}{4}, \frac{3}{2})$. Hence, we have

$$\begin{aligned}(\widehat{\widehat{V}}_{xx})^k_{l+\frac{1}{2}} &= \frac{1}{2h^2}(\widehat{V}^k_{l+1} - 2\widehat{V}^k_l + \widehat{V}^k_{l-1}) + \frac{1}{4h}(\widehat{W}^k_{l+1} - \widehat{W}^k_{l-1}) + \frac{3}{2h^2}(\widehat{V}^k_{l+1} - \widehat{V}^k_{l-1} - 2h\widehat{W}^k_l)\\ &= V^k_{xx_{l+\frac{1}{2}}} + \eta\tau^2 V_{22} + O(\tau^2 h + \tau^2 h^2 + h^3)\end{aligned} \tag{28}$$

Likewise, we have

$$\begin{aligned}(\widehat{\widehat{V}}_{xx})^k_{l-\frac{1}{2}} &= \frac{1}{2h^2}(\widehat{V}^k_{l+1} - 2\widehat{V}^k_l + \widehat{V}^k_{l-1}) + \frac{1}{4h}(\widehat{W}^k_{l+1} - \widehat{W}^k_{l-1}) - \frac{3}{2h^2}(\widehat{V}^k_{l+1} - \widehat{V}^k_{l-1} - 2h\widehat{W}^k_l)\\ &= V^k_{xx_{l-\frac{1}{2}}} + \eta\tau^2 V_{22} + O(\tau^2 h + \tau^2 h^2 + h^3)\end{aligned} \tag{29}$$

$$\begin{aligned}(\widehat{\widehat{W}}_{xx})^k_{l\pm\frac{1}{2}} &= -\frac{15}{4h^3}(\widehat{V}^k_{l+1} - \widehat{V}^k_{l-1} - 2h\widehat{W}^k_l) + \frac{9}{4h^2}(\widehat{W}^k_{l+1} + \widehat{W}^k_{l-1} - 2\widehat{W}^k_l) \mp \frac{6}{h^3}(\widehat{V}^k_{l+1} + \widehat{V}^k_{l-1} - 2\widehat{V}^k_l)\\ &\quad \pm \frac{3}{h^2}(\widehat{W}^k_{l+1} - \widehat{W}^k_{l-1})\\ &= W^k_{xx_{l\pm\frac{1}{2}}} + \eta\tau^2 V_{32} + O(\tau^2 h + \tau^2 h^2 + h^3)\end{aligned} \tag{30}$$

Employing the approximations (26.1)-(26.3) and (28)-(30), we define the additional functional approximation at the half-step points:

$$\widehat{\widehat{\Phi}}^k_{l\pm\frac{1}{2}} = \phi(x_{l\pm\frac{1}{2}}, t_j, \widehat{\widehat{V}}^k_{l\pm\frac{1}{2}}, \widehat{\widehat{V}}^k_{t_{l\pm\frac{1}{2}}}, \widehat{\widehat{W}}^k_{l\pm\frac{1}{2}}, \widehat{\widehat{V}}^k_{xx_{l\pm\frac{1}{2}}}, \widehat{\widehat{W}}^k_{xx_{l\pm\frac{1}{2}}}) = \Phi^k_{l\pm\frac{1}{2}} + O(\tau^2 + \tau^2 h + h^3) \tag{31}$$

Then, the difference method of $O(\tau^2 + h^4)$ for the differential equation (1) and the corresponding difference scheme for $w(x,t)$ maybe written as

$$\begin{aligned}&\left[a^k_l - \frac{2h^2}{15}\left(\frac{a^k_{x_l}}{a^k_l}\right)a^k_{x_l} + \frac{h^2}{15}a^k_{xx_l}\right]\left[-2(\widehat{V}^k_{l-1} - 2\widehat{V}^k_l + \widehat{V}^k_{l+1}) + h(\widehat{W}^k_{l+1} - \widehat{W}^k_{l-1})\right]\\ &+\frac{h^4}{90}\left[\left(1 - h\frac{a^k_{x_l}}{a^k_l}\right)(\widehat{V}_{tt})^k_{l+1} + 13(\widehat{V}_{tt})^k_l + \left(1 + h\frac{a^k_{x_l}}{a^k_l}\right)(\widehat{V}_{tt})^k_{l-1}\right]\\ &= \frac{h^4}{90}\left[\left(4 - 2h\frac{a^k_{x_l}}{a^k_l}\right)\widehat{\widehat{\Phi}}^k_{l+\frac{1}{2}} + 7\widehat{\widehat{\Phi}}^k_l + \left(4 + 2h\frac{a^k_{x_l}}{a^k_l}\right)\widehat{\widehat{\Phi}}^k_{l-\frac{1}{2}}\right] + \widehat{T}^{k^{(1)}}_l,\ l = 1, \ldots, N,\ k = 1, 2, \ldots\end{aligned} \tag{32a}$$

$$\begin{aligned}&a^k_l\left[-3(\widehat{V}^k_{l+1} - \widehat{V}^k_{l-1}) + h(\widehat{W}^k_{l-1} + 4\widehat{W}^k_l + \widehat{W}^k_{l+1})\right] + \frac{h^4}{60}\left[(\widehat{V}_{tt})^k_{l+1} - (\widehat{V}_{tt})^k_{l-1} - 2h\left(\frac{a^k_{x_l}}{a^k_l}\right)(\widehat{V}_{tt})^k_l\right]\\ &= \frac{h^4}{30}\left[\widehat{\Phi}^k_{l+\frac{1}{2}} - \widehat{\Phi}^k_{l-\frac{1}{2}} - h\left(\frac{a^k_{x_l}}{a^k_l}\right)\widehat{\Phi}^k_l\right] + \widehat{T}^{k^{(2)}}_l,\ l = 1, \ldots, N,\ k = 1, 2, \ldots\end{aligned} \tag{32b}$$

respectively, where $\widehat{T}_l^{k(1)} = O(\tau^2 h^4 + h^8)$ and $\widehat{T}_l^{k(2)} = O(\tau^2 h^5 + h^7)$, for arbitrary η. The Taylors expansion yield

$$\left[a_l^k - \frac{2h^2}{15}\left(\frac{a_{x_l}^k}{a_l^k}\right)a_{x_l}^k + \frac{h^2}{15}a_{xx_l}^k\right]\left[-2(V_{l-1}^k - 2V_l^k + V_{l+1}^k) + h(W_{l+1}^k - W_{l-1}^k)\right]$$
$$+\frac{h^4}{90}\left[\left(1 - h\frac{a_{x_l}^k}{a_l^k}\right)V_{tt_{l+1}}^k + 13V_{tt_l}^k + \left(1 + h\frac{a_{x_l}^k}{a_l^k}\right)V_{tt_{l-1}}^k\right]$$
$$= \frac{h^4}{90}\left[\left(4 - 2h\frac{a_{x_l}^k}{a_l^k}\right)\Phi_{l+\frac{1}{2}}^k + 13\Phi_l^k + \left(4 + 2h\frac{a_{x_l}^k}{a_l^k}\right)\Phi_{l-\frac{1}{2}}^k\right] + O(h^8) \tag{33a}$$

$$a_l^k\left[-3(V_{l+1}^k - V_{l-1}^k) + h(W_{l-1}^k + 4W_l^k + W_{l+1}^k)\right] + \frac{h^4}{60}\left[V_{tt_{l+1}}^k - V_{tt_{l-1}}^k - 2h\left(\frac{a_{x_l}^k}{a_l^k}\right)V_{tt_l}^k\right]$$
$$= \frac{h^4}{30}\left[\Phi_{l+\frac{1}{2}}^k - \Phi_{l-\frac{1}{2}}^k - h\left(\frac{a_{x_l}^k}{a_l^k}\right)\Phi_l^k\right] + O(h^7) \tag{33b}$$

Implementing the approximations (16.1)-(16.2), (16.4), (25), (31) in (32a) and with the help of relation (33a) and the governing differential (1), the local truncation error $\widehat{T}_l^{k(1)}$ associated with the difference method (32a) is obtained as

$$\widehat{T}_l^{k(1)} = \frac{h^6}{90}\left[a_{xx_l}^k\left(\frac{\partial^4 V}{\partial x^4}\right)_l^k + a_l^k\left(\frac{\partial^6 V}{\partial x^6}\right)_l^k + \left(\frac{\partial^4 V}{\partial x^2 \partial t^2}\right)_l^k - 2\frac{a_{x_l}^k}{a_l^k}\left(a_{x_l}^k\left(\frac{\partial^4 V}{\partial x^4}\right)_l^k + \left(\frac{\partial^3 V}{\partial x \partial t^2}\right)_l^k\right)\right.$$
$$\left. -\phi_{xx_l}^k + 2\frac{a_{x_l}^k}{a_l^k}\phi_{x_l}^k\right] + O(\tau^2 h^4 + h^8) \tag{34}$$

Differentiating (1) twice successively with respect to x and employing those relations in (34), the coefficient of h^6 in (34) vanishes and thus, the local truncation error is achieved as $\widehat{T}_l^{k(1)} = O(\tau^2 h^4 + h^8)$, for all choice of η. Similarly, $\widehat{T}_l^{k(2)} = O(\tau^2 h^5 + h^7)$ and thus the difference method (32b) is an approximation of order $O(\tau^2 h^2 + h^4)$ for the first-order spatial derivative $\frac{\partial v}{\partial x}(x,t) = w(x,t)$.

Including the given boundary and initial conditions, the three-point compact difference method results in block tridiagonal matrix form which is solved by applying appropriate iterative techniques. Block Gauss-Seidel iteration method can be applied if differential equation is linear while Newton's nonlinear block iteration method (see Kelly [17], Hageman and Young [13]) can be used for the nonlinear case.

The difference formulas (32a)-(32b) are free from the terms $1/x_{l\pm 1}$, hence solvable for $l = 1, \ldots, N$ for $0 < x < 1$, $t > 0$. The half-step nodes facilitate the direct application of the scheme (32a)-(32b) to problems with singularities without any modifications which is an advantage of the present method.

3 Stability investigation

For examining the stability, let us consider a linear parabolic PDE of fourth order:

$$\frac{\partial^4 v}{\partial x^4} + \frac{\partial^2 v}{\partial t^2} = \phi(x,t), \quad (x,t) \in \Omega \tag{35}$$

Implementing the finite difference method (32a)-(32b) of accuracy $O(\tau^2 + h^4)$ to the model (35), we get the following matrix form relating the mesh point values along the $(k+1)$th, kth and $(k-1)$th time rows:

$$\boldsymbol{P}\boldsymbol{y}^{(k+1)} = (2\boldsymbol{P} + \boldsymbol{Q})\boldsymbol{y}^{(k)} - \boldsymbol{P}\boldsymbol{y}^{(k-1)} + \boldsymbol{l} \tag{36}$$

where

$$\boldsymbol{P} = \begin{bmatrix} \boldsymbol{P}_{11} & \boldsymbol{P}_{12} \\ \boldsymbol{P}_{21} & \boldsymbol{P}_{22} \end{bmatrix}, \quad \boldsymbol{Q} = \begin{bmatrix} \boldsymbol{Q}_{11} & \boldsymbol{Q}_{12} \\ \boldsymbol{Q}_{21} & \boldsymbol{Q}_{22} \end{bmatrix}, \quad \boldsymbol{y} = \begin{bmatrix} \boldsymbol{v} \\ \boldsymbol{w} \end{bmatrix}, \quad \boldsymbol{l} = \begin{bmatrix} \boldsymbol{l}_1 \\ \boldsymbol{l}_2 \end{bmatrix}.$$

$\boldsymbol{P}$ and $\boldsymbol{Q}$ in (36) are block tridiagonal matrices of order $2N$ while $\boldsymbol{y}$ and $\boldsymbol{l}$ are $2N$ component column vectors. The solution vector is denoted by $\boldsymbol{y}$ whereas the column vector $\boldsymbol{l}$ represents known boundary data and function values on the right hand side of the matrix (36). The matrices $\boldsymbol{P}$ and $\boldsymbol{Q}$ are composed of the submatrices whose values are given by

$\boldsymbol{P}_{11} = [1, 13, 1] - 180\lambda^2\eta[1, -2, 1]$, $\boldsymbol{P}_{12} = 90\lambda^2\eta h[-1, 0, 1]$, $\boldsymbol{P}_{21} = (1 - 180\lambda^2\eta)[-1, 0, 1]$,
$\boldsymbol{P}_{22} = 60\lambda^2\eta h[1, 4, 1]$, $\boldsymbol{Q}_{11} = 180\lambda^2[1, -2, 1]$, $\boldsymbol{Q}_{12} = -90\lambda^2 h[-1, 0, 1]$, $\boldsymbol{Q}_{21} = 180\lambda^2[-1, 0, 1]$,
$\boldsymbol{Q}_{22} = -60\lambda^2\eta h[1, 4, 1]$.

Here, $[p, q, r]$ represents tridiagonal matrix of order N with characteristic values $q + 2\sqrt{pr}\cos(2\psi)$, $\psi = (r\pi)/(2(N+1))$, $r = 1, \ldots, N$. Also, $\boldsymbol{v} = (v_1, v_2, \ldots, v_N)^T$ and $\boldsymbol{w} = (w_1, w_2, \ldots, w_N)^T$ are the solution vectors.

The eigenvalues of submatrices $\boldsymbol{P}_{11}$, $\boldsymbol{P}_{12}$, $\boldsymbol{P}_{21}$ and $\boldsymbol{P}_{22}$ are $15 - 4(1 - 180\lambda^2\eta)\sin^2\psi$, $180\lambda^2\eta h\cos(2\psi)i$, $2(1 - 180\lambda^2\eta)\cos(2\psi)i$ and $120\lambda^2\eta h(3 - 2\sin^2\psi)$, respectively, where $i = \sqrt{-1}$.

Further, the eigenvalues of $\boldsymbol{Q}_{11}$, $\boldsymbol{Q}_{12}$, $\boldsymbol{Q}_{21}$ and $\boldsymbol{Q}_{22}$ are $-720\lambda^2\sin^2\psi$, $-180\lambda^2 h\cos(2\psi)i$, $360\lambda^2\cos(2\psi)i$ and $-120\lambda^2\eta h(3 - 2\sin^2\psi)$, respectively.

We examine the stability of differential equation (35) by considering the homogenous part of the difference scheme (36) written as

$$\boldsymbol{y}^{(k+1)} = (2\boldsymbol{I} + \boldsymbol{P}^{-1}\boldsymbol{Q})\boldsymbol{y}^{(k)} - \boldsymbol{I}\boldsymbol{z}^{(k)}, \tag{37.1}$$

$$\boldsymbol{z}^{(k+1)} = \boldsymbol{I}\boldsymbol{y}^{(k)} + \boldsymbol{0}\boldsymbol{z}^{(k)}. \tag{37.2}$$

Let us denote $\epsilon_1^{(k)} = \boldsymbol{y}^{(k)} - \boldsymbol{Y}^{(k)}$ and $\epsilon_2^{(k)} = \boldsymbol{z}^{(k)} - \boldsymbol{Z}^{(k)}$ (in the absence of round-off errors) the error vectors at the kth iterate, where

$$\boldsymbol{Z}^{(k+1)} = \boldsymbol{Y}^{(k)} = \begin{bmatrix} \boldsymbol{V} \\ \boldsymbol{W} \end{bmatrix}^{(k)},$$

$\boldsymbol{V}$ and $\boldsymbol{W}$ are exact solution vectors. With this, the error equation becomes

$$\mathbf{E}^{(k+1)} = \begin{bmatrix} \epsilon_1^{(k+1)} \\ \epsilon_2^{(k+1)} \end{bmatrix} = \boldsymbol{H}\mathbf{E}^{(k)},$$

for the amplification matrix $\boldsymbol{H}$ given by

$$\boldsymbol{H} = \begin{bmatrix} 2\boldsymbol{I} + \boldsymbol{P}^{-1}\boldsymbol{Q} & -\boldsymbol{I} \\ \boldsymbol{I} & \boldsymbol{0} \end{bmatrix}.$$

The eigenvalue χ of the matrix $\boldsymbol{P}$ satisfies the below characteristic equation:

$$\det\begin{bmatrix} 15 - 4(1 - 180\lambda^2\eta)\sin^2\psi - \chi & 180\lambda^2\eta h\cos(2\psi)i \\ 2(1 - 180\lambda^2\eta)\cos(2\psi)i & 120\lambda^2\eta h(3 - 2\sin^2\psi) - \chi \end{bmatrix} = 0 \tag{38}$$

The eigenvalue ξ of the matrix $\boldsymbol{Q}$ satisfies the below characteristic equation:

$$\det\begin{bmatrix} -720\lambda^2\sin^2\psi - \xi & -180\lambda^2 h\cos(2\psi)i \\ 360\lambda^2\cos(2\psi)i & -120\lambda^2\eta h(3 - 2\sin^2\psi) - \xi \end{bmatrix} = 0 \tag{39}$$

Let ω denote the eigenvalue of $\boldsymbol{P}^{-1}\boldsymbol{Q}$. The characteristic equation satisfied by the eigenvalue ρ of the amplification matrix $\boldsymbol{H}$ can be written as

$$\det\begin{bmatrix} 2 + \omega - \rho & -1 \\ 1 & -\rho \end{bmatrix} = 0$$

which yields

$$\rho^2 - 2\gamma\rho + 1 = 0 \tag{40}$$

for $\gamma = 1 + \frac{\omega}{2}$. Thus, the difference scheme (37.1)-(37.2) is stable provided $|\gamma| \leq 1$, that is,

$$-4 \leq \omega \leq 0. \tag{41}$$

The characteristic equations (38) and (39) can be written as

$$\chi^2 - (r_1 + s_2)\chi + (r_1 s_2 - s_1 r_2) = 0$$
$$\xi^2 - (r_3 + s_4)\xi + (r_3 s_4 - s_3 r_4) = 0$$

respectively, where

$$\begin{aligned}
r_1 &= 15 - 4(1 - 180\lambda^2\eta)\sin^2\psi, \\
r_2 &= 180i\lambda^2\eta h\cos(2\psi), \\
r_3 &= -720\lambda^2\sin^2\psi, \\
r_4 &= -180i\lambda^2 h\cos(2\psi), \\
s_1 &= 2i(1 - 180\lambda^2\eta)\cos(2\psi), \\
s_2 &= 120\lambda^2\eta h(3 - 2\sin^2\psi), \\
s_3 &= 360i\lambda^2\cos(2\psi), \\
s_4 &= -120\lambda^2\eta h(3 - 2\sin^2\psi).
\end{aligned}$$

Thus, the above quadratic equations give the eigenvalues of $\boldsymbol{P}$ and $\boldsymbol{Q}$ as

$$\chi_{1,2} = \frac{1}{2}\left[(r_1 + s_2) \pm \sqrt{(r_1 - s_2)^2 + 4s_1 r_2}\right] \tag{42}$$

and

$$\xi_{1,2} = \frac{1}{2}\left[(r_3 + s_4) \pm \sqrt{(r_3 - s_4)^2 + 4s_3 r_4}\right] \tag{43}$$

respectively. The eigenvalues of the product $\boldsymbol{P}^{-1}\boldsymbol{Q}$ are given by $\dfrac{\xi_{1,2}}{\chi_{1,2}}$ since the matrices $\boldsymbol{P}^{-1}$ and $\boldsymbol{Q}$ commute. Hence, from (41), we obtain the relation

$$\xi_{1,2} + 4\chi_{1,2} \geq 0 \tag{44}$$

For small h, condition (44) holds if $r_3 + 4r_1 \geq 0$, i.e., if

$$(2880\eta - 720)\lambda^2 \sin^2\psi + 4(15 - 4\sin^2\psi) \geq 0$$

which is true if $2880\eta - 720 \geq 0$. Hence, condition (44) is satisfied for all choices of $\lambda > 0$ provided $\eta \geq \frac{1}{4}$. Thus, the difference scheme (36) is stable for $\eta \geq \frac{1}{4}$.

4 Numerical experiments

For examining the accuracy of the derived method, we have determined the solution of various linear and nonlinear parabolic problems of fourth order having physical significance. We have taken standard problems widely considered in the literature for testing different methods as numerical examples. For computations, $\eta = 0.5$ has been chosen for each problem. The proposed difference formulas yield block tridiagonal matrices. We have applied Gauss-Seidel iteration method for determining the solution of coupled linear system of equations while Newton's nonlinear method has been applied for solving nonlinear equations (see [17, 24]). In all cases, we have terminated the iterations when the absolute error tolerance $1e-10$ has been attained.

Note that the difference method (32a)–(32b) for the solution of equation (1) is a three time-level method. The solution values v and w are known at $t = 0$ from the initial conditions. At first time-level $t = \tau$, the solution values v and w of desired accuracy are needed for beginning the computation, for which we employ an explicit difference method of accuracy $O(\tau^2)$ that is applicable to problems in cartesian and polar coordinates. Using the known initial values of v and $\partial v/\partial t$, the following consecutive tangential derivatives are known at $t = 0$:

$$\frac{\partial^q v_l^0}{\partial x^q},\ \frac{\partial^q w_l^0}{\partial x^q},\ \frac{\partial^{q+1} v_l^0}{\partial x^q \partial t},\ \frac{\partial^{q+1} w_l^0}{\partial x^q \partial t},\quad q = 0, 1, \ldots$$

The given differential (1) may be re-written as:

$$\frac{\partial^2 v}{\partial t^2} = -a(x,t)\frac{\partial^4 v}{\partial x^4} + \phi(x,t,v,v_t,w,v_{xx},w_{xx}) \tag{45}$$

Differentiating (45) with respect to x, we get

$$\frac{\partial^2 w}{\partial t^2} = -a\frac{\partial^4 w}{\partial x^4} - a_x\frac{\partial^4 v}{\partial x^4} + \frac{\partial \phi}{\partial x} + \frac{\partial \phi}{\partial v}\frac{\partial v}{\partial x} + \frac{\partial \phi}{\partial v_t}\frac{\partial^2 v}{\partial x \partial t} + \frac{\partial \phi}{\partial w}\frac{\partial w}{\partial x} + \frac{\partial \phi}{\partial v_{xx}}\frac{\partial^3 v}{\partial x^3} + \frac{\partial \phi}{\partial w_{xx}}\frac{\partial^3 w}{\partial x^3} \tag{46}$$

The following explicit difference schemes of accuracy $O(\tau^2)$ are used for the solution values v and w at first time-level:

$$V_l^1 = V_l^0 + \tau V_{t_l}^0 + \frac{\tau^2}{2} V_{tt_l}^0 + O(\tau^3) \tag{47}$$

$$W_l^1 = W_l^0 + \tau W_{t_l}^0 + \frac{\tau^2}{2} W_{tt_l}^0 + O(\tau^3) \tag{48}$$

Hence, considering the initial and consecutive tangential derivative values, the values of $V_{tt_l}^0$ and $W_{tt_l}^0$ are obtained from (45) and (46), respectively. Furthermore, these values are substituted in (47) and (48) for computing v and w at first time-level.

To demonstrate the accuracy of the proposed method, we evaluate the error norms defined as below:

$$L_\infty = \max_{1 \le l \le N} |v(x_l,t) - V(x_l,t)|,$$

$$L_2 = \left[\frac{1}{N}\sum_{l=1}^{N} |v(x_l,t) - V(x_l,t)|^2\right]^{1/2},$$

To validate the efficacy of the derived scheme and for comparing it with the available methods, we examined the propagation of solitary wave for the good Boussinesq equation and report numerical findings for different time and space steps. Then, we investigated the interaction of two solitary waves.

Example 1 [21, 25] (*Euler-Bernoulli beam equation*)
Consider the following dynamic Euler-Bernoulli problem:

$$\frac{\partial^2 v}{\partial t^2} + \frac{\partial^2}{\partial x^2}\left((1+\sin \pi x)\frac{\partial^2 v}{\partial x^2}\right) = \phi(x,t), \quad 0 < x < 1, \quad t > 0, \tag{49}$$

with the exact solution $v(x,t) = x(1-x)e^{-t}t^2 \sin 4\pi x$ and the forcing function $\phi(x,t)$ is dictated by the exact solution. Applying the present scheme (32a)-(32b), we report and compare absolute errors in the computed solution at the point $x = 0.5$ for different times in Table 1 using $N = 50, 100, 200$ and time stepsize $\tau = 0.1$ and 0.01 with the sextic B-spline collocation method proposed in [21]. It can be observed from Table 1 that the numerical errors in the solution by the present method are less than the available methods. Figure 1 displays surface plots of the numerical and exact solutions from $t = 0$ to 4.

Table 1 Comparison of L_∞ errors at different times for various values of τ and N at $x = 0.5$, Example 1

Methods	τ	N	$t = 0.2$	$t = 0.4$	$t = 0.8$	$t = 1.0$	$t = 2.0$	$t = 4.0$
Present method	0.1	50	3.0299e−006	2.4198e−006	2.6963e−006	2.5918e−006	2.0809e−006	1.5943e−006
		100	1.2191e−007	1.1985e−008	5.4931e−008	5.1510e−008	9.8116e−008	2.9845e−008
		200	7.2283e−010	4.0861e−009	1.0675e−008	1.2306e−008	1.6321e−008	8.3796e−009
	0.01	50	5.9554e−008	9.6068e−008	2.4116e−007	3.1462e−007	4.6266e−007	2.4925e−007
		100	2.8983e−009	9.9566e−009	2.6185e−008	3.3292e−008	4.8291e−007	2.6088e−008
		200	1.0572e−009	3.3182e−009	8.6759e−009	1.1039e−008	1.6072e−008	8.6610e−009
Method[21]	0.1	50	1.03e−004	3.38e−004	9.08e−004	1.16e−003	1.70e−003	9.25e−004
		100	1.79e−005	5.85e−005	1.57e−004	2.01e−004	2.95e−004	1.60e−004
		200	2.38e−006	7.80e−006	2.09e−005	2.67e−005	3.93e−005	2.13e−005
	0.01	50	1.03e−004	3.38e−004	9.09e−004	1.16e−003	1.80e−003	9.51e−004
		100	1.78e−005	5.85e−005	1.57e−004	2.00e−004	2.95e−004	1.60e−004
		200	2.37e−006	7.80e−006	2.09e−005	2.67e−005	3.93e−005	2.13e−005

Example 2 [5–7, 10, 14, 28, 29] (*Solitary wave propagation*)
In this experiment, we consider the good Boussinesq (5) on the interval $[x_a, x_b] = [-100, 140]$. Its well-known soliton solution as obtained by Manoranjan et al. [18] is

$$v(x,t) = -A\,\mathrm{sech}^2\left[\sqrt{\frac{A}{6}}(x - ct + x^0)\right] - \left(b + \frac{1}{2}\right) \tag{50}$$

where A is amplitude of the pulse, $c = \pm\left[-2\left(b + \frac{A}{3}\right)\right]^{1/2}$ is the velocity of the solitary wave, x^0 is the initial position of the pulse and b is an arbitrary parameter. The exact solution (50) represents a solitary wave progressing to the right (to the left) if the velocity c is positive (negative). The initial conditions can be procured from the exact solution. The boundary constraints are obtained graphically by the nature of the exact propagating wave solution as the time evolves. The analytical solution die away along the boundaries of the physical domain. Consequently, the boundary conditions are

$$\begin{aligned} &v(x_a,t) = 0, \qquad v(x_b,t) = 0, \quad t > 0,\\ &\frac{\partial v}{\partial x}(x_a,t) = 0, \quad \frac{\partial v}{\partial x}(x_b,t) = 0, \quad t > 0. \end{aligned}$$

For comparison with the existing methods, we select the parameters A, b and x^0 as in [10, 14], i.e. $A = 0.369$, $b = -0.5$ and $x^0 = 0$. Table 2 presents comparison of L_∞ and L_2 error norms using the derived method with $h = 0.1$, $\tau = 0.01$ with those in [10, 14]. Furthermore, we solve Eq. (5) at several time-levels using different space and time steps and compare with the existing numerical methods in Table 3. As depicted by the tables, the numerical results using the present method are more accurate than those derived in earlier studies [5, 7, 10, 14, 28, 29] even for longer time periods. The comparisons with respect to the energy-preserving methods just look at the solution error of the solution at different times since the preservation/non-

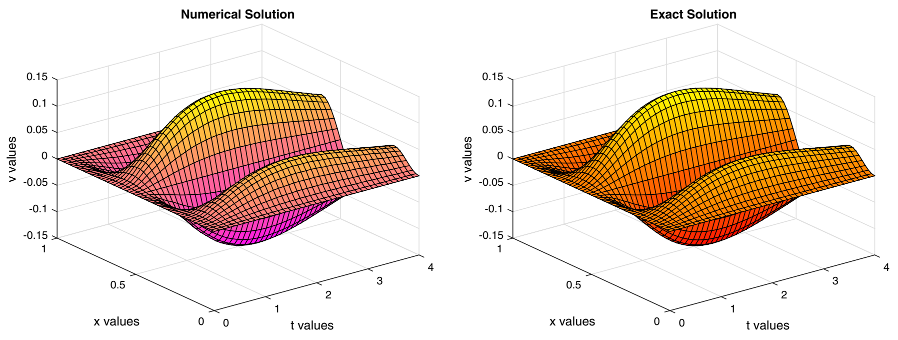

(a) Numerical Solution (b) Exact Solution

Fig. 1 The surface plot of numerical and exact solutions from $t = 0$ to 4 with $N = 50$ and $\tau = 0.1$, Example 1

Table 2 Comparison of L_∞ and L_2 errors at different times with $h = 0.1$ and $\tau = 0.01$, Example 2 for $A = 0.369$, $x^0 = 0$

t	Present method L_2	Present method L_∞	Method [10] L_2	Method [10] L_∞	Method [14] L_2	Method [14] L_∞
10	6.3149e−011	5.6312e−010	4.0150e−006	2.1346e−002	8.0000e−006	1.0000e−006
20	2.1866e−010	2.2719e−009	-	-	1.3000e−005	2.0000e−006
30	3.7768e−010	3.8776e−009	4.0260e−006	2.8142e−002	1.7000e−005	2.0000e−006
40	5.5913e−010	5.7058e−009	-	-	2.0000e−005	3.0000e−006
50	6.8809e−010	7.1155e−009	-	-	2.3000e−005	3.0000e−006
60	9.4285e−010	9.5739e−009	4.0011e−006	5.6516e−003	-	-

Table 3 Solitary wave motion. A comparison of L_∞ errors for the proposed method and available methods [5–7, 10, 14, 28, 29], Example 2 at different times for various values of h and τ

Method	h	τ	t	L_∞
Method	h	τ	t	L_∞
Proposed method	0.5	0.01	30	4.0200e−005
	0.5	0.01	36	5.3765e−005
	0.5	0.01	60	1.2576e−004
	0.5	0.01	72	1.7259e−004
	0.1	0.01	30	3.8776e−009
	0.1	0.01	36	5.4712e−009
	0.1	0.01	60	9.5739e−009
	0.1	0.01	72	1.1479e−008
	0.5	0.01	80	2.2766e−004
	0.1	0.01	80	1.3088e−008
Nonlinear method [14]	0.1	0.001	72	9.7000e−008
Galerkin method [28]	0.5	0.002	30	3.274e−006
	0.1	0.002	30	2.4854e−005
	0.5	0.002	60	5.033e−006
	0.1	0.002	60	4.2511e−005
	0.1	0.001	72	8.814e−006
Linearized scheme [14]	0.1	0.001	72	9.7500e−004
Energy preserving scheme [7]	0.05	0.001	36	5.9926e−005
	0.05	0.001	72	9.0146e−005
Multiquadric method [29]	0.5	0.0002	72	2.205e−005
Second-order P-C scheme [5]	0.1	0.001	72	3.7799e−004
	0.05	0.001	72	1.0687e−004
Meshless method [10]	–	–	30	2.8141e−002
			36	4.7325e−003
			60	5.6516e−003
			72	4.8863e−004

preservation of the invariants of motions is beyond the scope of the manuscript. The 2D plot of approximate solution versus exact solution is presented in Fig. 2 at different times with $h = 0.1$ and $\tau = 0.01$. It is depicted that the shape of the solitary wave is retained extremely well at each time-level.

Example 3 [1, 5, 7, 10, 14, 29] (*Interaction of two solitary waves*)

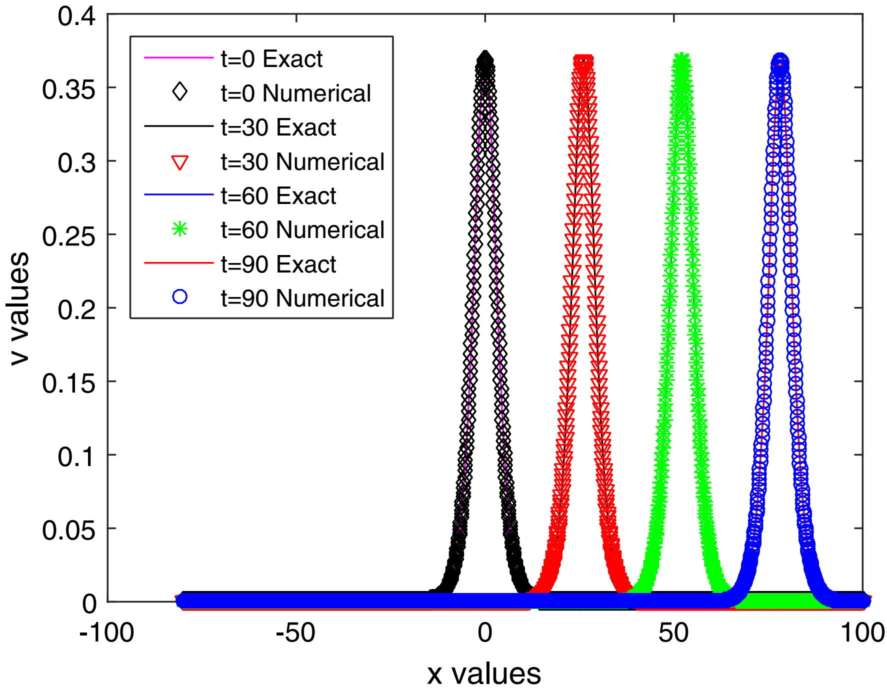

Fig. 2 Comparison between numerical and exact solution at different times with $h = 0.1$, $\tau = 0.01$, Example 2

Consider the Boussinesq (5) with the following exact solution:

$$v(x,t) = -\sum_{i=1}^{2}\left\{A_i \operatorname{sech}^2\left[\sqrt{\frac{A_i}{6}}(x - c_i t + x_i^0)\right] + b_i + \frac{1}{2}\right\} \tag{51}$$

where $c_i = \pm\left[-2\left(b_i + \frac{A_i}{3}\right)\right]^{1/2}$; $i = 1, 2$ are the velocities of the ith solitary, A_i, $i = 1, 2$ are the corresponding amplitudes of the pulse and b_i, $i = 1, 2$ are arbitrary parameters. The exact solution (51) exhibits two solitary waves positioned initially at x_i^0, $i = 1, 2$ and progressing to the right or left depending on the sign of the velocity

Table 4 Error norms L_∞ of obtained numerical solution of double-soliton case, Example 3 (i) for $A_1 = 0.369,\ A_2 = 0.369,\ x_1^0 = 0,\ x_2^0 = 50$ at $t = 10$

Method	h	τ	L_∞
Present method (32a)-(32b)	0.5	0.1	5.5852e−003
	0.5	0.01	5.7832e−003
	0.25	0.1	5.6195e−003
	0.25	0.01	5.7955e−003
Method [10]	–	–	2.1016e−002

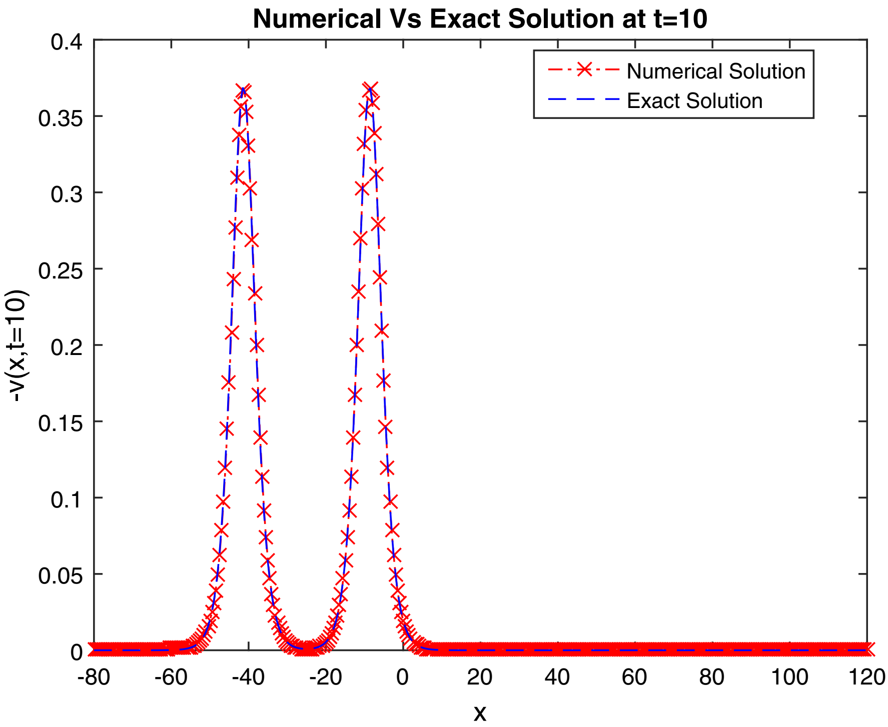

Fig. 3 Plot of numerical and exact solutions at $t = 10$, Example 3 (i), case of equal amplitudes $A_1 = A_2 = 0.369$

c_i, $i = 1, 2$. We investigate the double-soliton solution by examining following two cases:

(i) Simulations are carried out for $-80 \leq x \leq 120$ and $0 \leq t \leq 10$ to find approximate solution of two waves with equal amplitudes $A_1 = A_2 = 0.369$ located initially at $x_1^0 = 0$ and $x_2^0 = 50$ and traveling towards each other with velocities $-c_1 = c_2 = 0.868$ for $b_1 = b_2 = -0.5$ with different values of h and τ. The L_∞ errors between the exact solution and approximate solution obtained by the known studied methods and the present method are recorded in Table 4.

Table 5 Error norms L_∞ of obtained numerical solution for double-soliton case, Example 3 (ii) for $A_1 = 0.2,\ A_2 = 0.4,\ x_1^0 = 0,\ x_2^0 = 50$ at $t = 10$

Method	h	τ	L_∞
Present method (32a)-(32b)	0.5	0.1	2.9015e−004
	0.5	0.01	4.1856e−005
	0.25	0.1	2.9792e−004
	0.25	0.01	4.8714e−005
	0.1	0.01	6.9307e−008
Method [10]	–	–	1.4563e−002

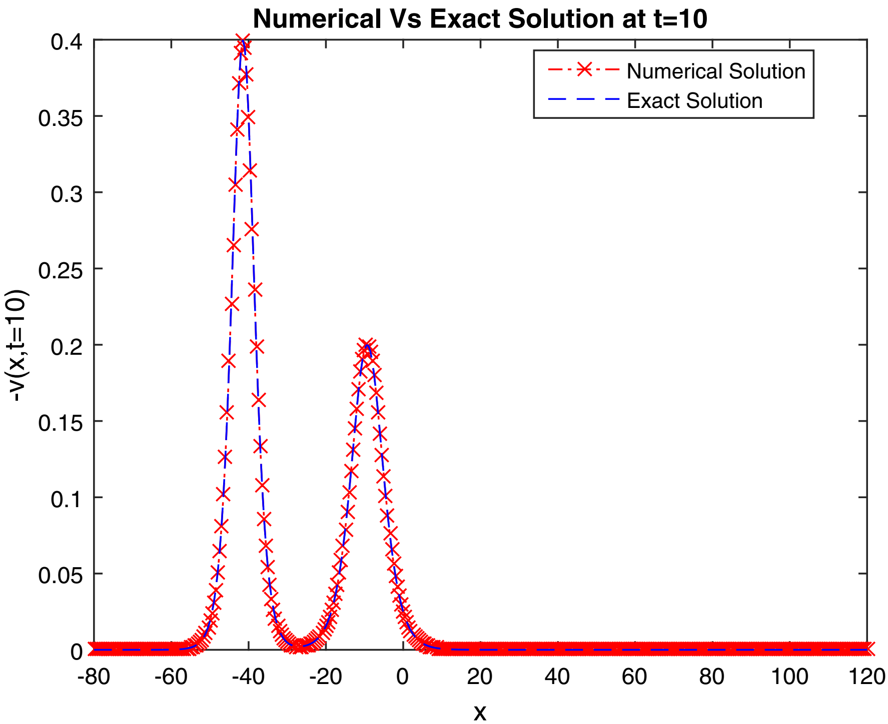

Fig. 4 Comparison between numerical and exact solution at $t = 10$, Example 3 (ii) with different amplitudes $A_1 = 0.2$, $A_2 = 0.4$

In Fig. 3, two-dimensional plots of numerical and exact solution are depicted at $t = 10$.

(ii) Computations are done for $-80 \le x \le 12$ and from time $0 \le t \le 10$ with different space and time steps for two waves having different amplitudes $A_1 = 0.2$, $A_2 = 0.4$ traveling towards each other with velocities $c_1 = -0.9309$, $c_2 = 0.8563$ positioned initially at $x_1^0 = 0$ and $x_2^0 = 50$ for $b_1 = b_2 = -0.5$. Comparison of the obtained numerical results using the proposed method

Table 6 Error norms L_∞ of obtained numerical solution of double-soliton case, Example 3 (ii) for $A_1 = 0.2$, $A_2 = 0.4$, $x_1^0 = -20$, $x_2^0 = 20$ at various times

t	Present method (32a)–(32b)		Method [1]
	$h = 0.1,\ \tau = 0.01$	$h = 0.05,\ \tau = 0.01$	
0.5	1.1663e−010	3.0638e−012	5.7911e−009
2.0	1.0668e−010	3.3609e−012	1.2203e−007
5.0	1.8669e−009	7.6461e−012	1.5596e−006
10	1.5346e−005	5.4495e−011	–
15	1.1107e−003	–	1.1558e−003

with the existing method[10] is presented in Table 5. Figure 4 represents the two-dimensional plot of numerical solution versus exact solution at $t = 10$. Furthermore, we examine the double-soliton solutions with $A_1 = 0.2$, $A_2 = 0.4$ positioned initially at $x_1^0 = -20$ and $x_2^0 = 20$ for $b_1 = b_2 = -0.5$ and compared our results with [1] for $x \in [-80, 100]$ and $0 \le t \le 15$ with space step $h = 0.1$, 0.05; time step $\tau = 0.01$ in Table 6. The numerical results reveal that our compact scheme performs better than the method proposed in [1].

Example 4 [25] Let us examine the following parabolic equation of fourth order:

$$\frac{\partial^4 v}{\partial x^4} + \frac{\partial^2 v}{\partial t^2} = \phi(x, t), \quad 0 < x < 1, \ t > 0 \tag{52}$$

with the initial conditions (2.1)-(2.2) and boundary conditions of the kind (3.1)-(3.2) whose exact solution is

$$v(x, t) = [x(1 - x)]^{7/2} t^{5/2} e^{-t}.$$

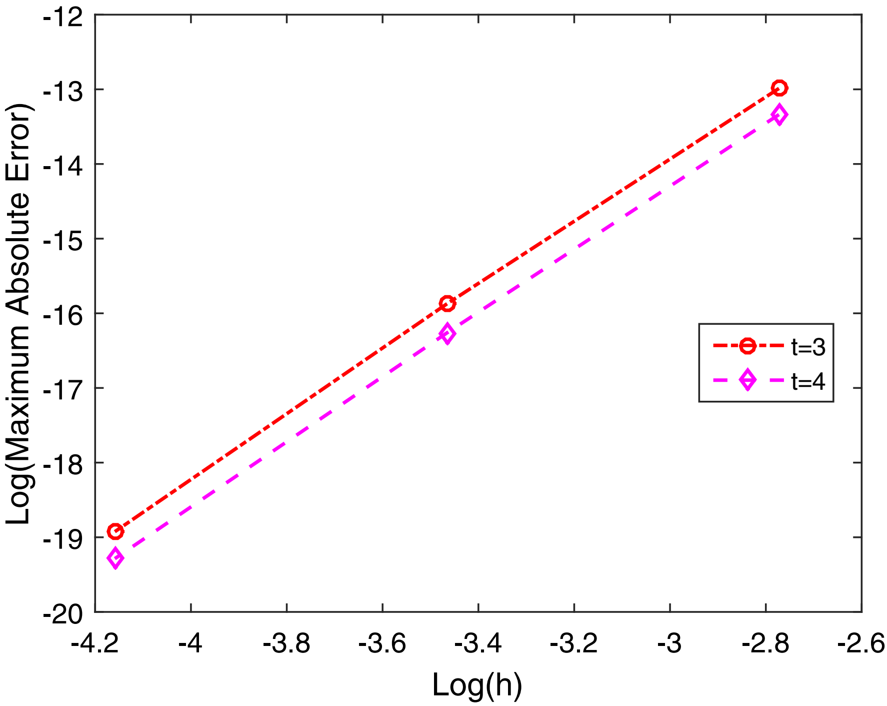

Fig. 5 Error plots for Example 4 at $t = 3$ and $t = 4$ with $\lambda = 1.6$

and

$$\phi(x,t) = \frac{e^{-t}\sqrt{t}\left(60(x-1)^4x^4 - 80t(x-1)^4x^4 + t^2\left(105 - 3360x + 16800x^2 - 26880x^3 + 13456x^4 - 64x^5 + 96x^6 - 64x^7 + 16x^8\right)\right)}{16\sqrt{x\,(1-x)}}$$

At points $x = 0$ and $x = 1$, the function $\phi(x,t)$ has algebraic singularities. We compute the solution at $t = 3, 4$ with $N + 1 = 16, 32, 64$ for $\lambda = 1.6$ using the proposed difference scheme (32a)-(32b) and present L_∞ errors in solution in Fig. 5. Corresponding to each spatial step length h, we have taken the time step as $\tau \propto h^2$ so that the proposed method has order of convergence $O(h^4)$, i.e., it is fourth-order accurate in space. It is evident from Fig. 5 that the graph has almost constant slope around four.

5 Conclusions

The current study proposes a high-order compact numerical scheme based on half-step discretization for the general form of parabolic PDEs of fourth order with the Dirichlet and Neumann boundary conditions. The derived scheme exhibits fourth-order convergence in space and has second-order accuracy in time. We do not need any special approach/alteration for computing the solution in the proximity of the singular point unlike the method discussed in [16] wherein a special handling was needed leading to tedious calculations. By the use of half-step nodes, the proposed scheme is able to avoid the singularity and hence is directly applicable to parabolic problems of fourth order with singularities as illustrated by Example 4. We have analyzed the stability of the derived method for a model linear problem. Furthermore, the first-order spatial derivative is obtained together with the solution, and hence, it does not have to be approximated by the estimated value of the solution. The obtained numerical results exhibit reasonably small error norms L_2 and L_∞ as compared to the methods derived in previous studies for several benchmark physical problems. Extensive numerical tests are presented to validate the theoretical findings and to illustrate rich dynamics of the good Boussinesq equation by investigating the motion of a solitary wave and interaction of two solitary waves. The present method can also be applied for solving a wide class of diverse fourth order evolution equations in applied sciences and engineering. Future investigation will be conducted to extend the present approach to higher dimensional problems.

Acknowledgements We are thankful to Science and Engineering Research Board (SERB) (Sanction Order No.: CRG/2018/004608) for providing support during this research work.

Author Contributions In this work, all authors contributed equally.

Data availibility Because no datasets were collected or analyzed during the present investigation, data sharing is not applicable to this publication.

Declarations

Ethical approval There are no studies involving human participants or animals done by any of the authors in this article.

Conflict of interest The authors declare no competing interests.

References

1. Mohebbi, A., Asgari, Z.: Efficient numerical algorithms for the solution of "good" Boussinesq equation in water wave propagation. Comput. Phys. Comm. **182**, 2464–2470 (2011)
2. Almatrafi, M.B., Alharbi, A.R.: Tunç, Cemil: Constructions of the soliton solutions to the good Boussinesq equation. Adv. Difference Equ. Paper No. **629** (2020)
3. Boussinesq, M.J.: Theory of waves and vortices propagating along a horizontal rectangular channel, communicating to the liquid in the channel generally similar velocities of the bottom surface. J. Math. Pures Appl. **17**, 55–108 (1872)
4. Bratsos, A.G.: The solution of the Boussinesq equation using the method of lines. Comput. Methods Appl. Mech. Eng. **157**, 33–44 (1998)
5. Bratsos, A.G.: A second order numerical scheme for the solution of the one-dimensional Boussinesq equation. Numer. Algor. **46**, 45–58 (1872)
6. Brugnano, L., Gurioli, G., Zhang, C.: Spectrally accurate energy-preserving methods for the numerical solution of the "good" Boussinesq equation. Numer. Methods Partial. Differ. Equ. **35**, 1343–1362 (2019)
7. Cai, J., Wang, Y.: Local structure-preserving algorithms for the "good" Boussinesq equation. J. Comput. Phys. **239**, 72–89 (2013)
8. Chawla, M.M., Shivakumar, P.N.: An efficient finite difference method for two-point boundary value problems. Neural Parallel Sci. Comput. **4**, 387–395 (1996)
9. Chen, M., Kong, L., Hong, Y.: Efficient structure-preserving schemes for good Boussinesq equation. Math. Methods Appl. Sci. **41**, 1743–1752 (2018)
10. Dehghan, M., Salehi, R.: A meshless based numerical technique for traveling solitary wave solution of Boussinesq equation. Appl. Math. Model. **36**, 1939–1956 (2012)
11. El-Gamel, M.: A note on solving the fourth-order parabolic equation by the sinc-Galerkin method. Calcolo **52**, 327–342 (2015)
12. Gorman, D.G.: Free vibrations analysis of beams and shafts. Wiley, New York (1975)
13. Hageman, L.A., Young, D.M.: Applied iterative methods. Dover Publication, New York (2004)
14. Ismail, M.S., Mosally, F.: A fourth order finite difference method for the good Boussinesq equation. Abstr. Appl. Anal. Art. ID **323260**, 10 (2014)
15. Jiang, C., Sun, J., He, X., Zhou, L.: High order energy-preserving method of the "good" Boussinesq equation. Numer. Math. Theory Methods Appl. **9**, 111–122 (2016)
16. Kaur, D., Mohanty, R.K.: Highly accurate compact difference scheme for fourth order parabolic equation with Dirichlet and Neumann boundary conditions: Application to good Boussinesq equation. Appl. Math. Comput. **378**(125202) (2020)
17. Kelly, C.Y.: Iterative methods for linear and non-linear equations. SIAM Publications, Philadelphia (1995)
18. Manoranjan, V.S., Mitchell, A.R., Morris, JLl.: Numerical solutions of the good Boussinesq equation. SIAM J. Sci. Statist. Comput. **5**, 946–957 (1984)
19. Maruno, K., Biondini, G.: Resonance and web structure in discrete soliton systems: the two-dimensional Toda lattice and its fully discrete and ultradiscrete analogues. J. Phys. A: Math. Gen. **37**, 11819–11839 (2004)
20. Meirovitch, L.: Principles and techniques of vibrations. Prentice Hall, New Jersey (1997)
21. Mohammadi, R.: Sextic B-spline collocation method for solving Euler-Bernoulli beam models. Appl. Math. Comput. **241**, 151–166 (2014)
22. Mohanty, R.K., Kaur, D.: Unconditionally stable high accuracy compact difference schemes for multi-space dimensional vibration problems with simply supported boundary conditions Appl. Math. Model. **55**, 281–298 (2018)

23. Ostermann, A., Su, C.: Two exponential-type integrators for the "good" Boussinesq equation. Numer. Math. **143**, 683–712 (2019)
24. Saad, Y.: Iterative methods for sparse linear systems. SIAM Publisher (2003)
25. Smith, R.C., Bowers, K.L., Lund, J.: A fully sinc-Galerkin method for Euler-Bernoulli beam models. Numer. Methods Part. Differ. Equ. **8**, 171–202 (1992)
26. Soh, C.W.: Euler-Bernoulli beams from a symmetry standpoint-characterization of equivalent equations. J. Math. Anal. Appl. **45**, 387–395 (2008)
27. Su, C., Yao, W.: A Deuflhard-type exponential integrator Fourier pseudo-spectral method for the "good" Boussinesq equation. J. Sci. Comput. Paper No. 4, 83, 19 (2020)
28. Ucar, Y., Esen, A., Karaagac, B.: Numerical solutions of Boussinesq equation using Galerkin finite element method. Numer. Methods Part. Differ. Equ. **37**, 1612–1630 (2021)
29. Uddin, M., Haq, S., Ishaq, M.: RBF-pseudospectral method for the numerical solution of good Boussinesq equation. Appl. Math. Sci. (Ruse) **6**, 2403–2410 (2012)
30. Yan, J., Zhang, Z.: New energy-preserving schemes using Hamiltonian boundary value and Fourier pseudospectral methods for the numerical solution of the "good" Boussinesq equation Comput. Phys. Commun. **201**, 33–42 (2016)
31. Zhang, C., Huang, J., Wang, C., Yue, X.: On the operator splitting and integral equation preconditioned deferred correction methods for the "good" Boussinesq equation. J. Sci. Comput. **75**, 687–712 (2018)

Authors and Affiliations

Deepti Kaur[1] · R. K. Mohanty[2]

Deepti Kaur
deeptikaur@ms.du.ac.in

[1] Department of Mathematics, Mata Sundri College for Women, University of Delhi, Delhi 110002, India

[2] Department of Applied Mathematics, Faculty of Mathematics and Computer Science, South Asian University, Rajpur Road, Maidan Garhi, New Delhi 110068, India